J. Plasma Physics (2008), *vol.* 74, *part* 2, *pp.* 233–244. © 2008 Cambridge University Press
doi:10.1017/S0022377807006976 First published online 2 January 2008 Printed in the United Kingdom

Coaxial cavity vircator with enhanced efficiency

G.Z. LIU, H. SHAO, Z.F. YANG, Z.M. SONG, C.H. CHEN, J. SUN and Y.P. ZHANG

Northwest Institute of Nuclear Technology, Xi'an, China
(gzliu@nint.ac.cn)

(Received 23 March 2007 and in revised form 30 September 2007)

Abstract. A vircator with a coaxial cavity has the potential to increase the beam–microwave conversion efficiency. According to the E-field distribution pattern of the modes in the anode cavity of a coaxial vircator, the resonant frequency band of the injected electron beam and the lowest two operating modes are derived. The main frequency of the virtual cathode is also deduced. The optimal operating frequency and high-efficiency designing method of a coaxial cavity vircator is discussed. An experimental setup is designed and built to test the high-power microwave (HPM) generation mechanism described by theoretical analysis as well as increase the power efficiency. HPM frequency obtained in the experiment is in good agreement with the analysis. The power and energy efficiencies obtained in the experiment are, respectively, 8.7% and 6.8% with 50 ns pulse width. Frequency and phase stable HPM radiation is observed as well as pulse shortening is evidently depressed.

1. Introduction

The virtual cathode oscillator is an important branch of high-power microwave (HPM) generation. It is a strong nonlinear space-charge effect HPM device, in which HPM radiation is generated by the injected electron beam current exceeding the space-charge-limiting current of the drift cavity. With the capacity of generating an ultra-HPM pulse, its simple configuration and no need for a high-quality electron beam and cumbersome magnetic field supporting system, it had been focused on for nearly 30 years until it was found that the bottleneck of low efficiency was difficult to overcome [1, 2].

Over the past three decades, many novel types of vircator were designed to increase the beam–HPM power conversion efficiency, among which the coaxial vircator is a potential device to achieve the final goals. The prototype of the coaxial vircator was originally proposed and developed by Zherlitsyn [3], Guozhi Liu [4] and M. Kristiansen [5]. With a quasi-cavity configuration, the coaxial vircator has been proved to have the capacity of relative high efficiency and frequency-stable output compared with other virtual cathode oscillators [6–9]. To further increase the efficiency of the coaxial vircator, we should peer into the basic process of the electron beam interacting with cavity modes and obtain the design and optimized methods for the experimental configuration.

The interaction process between the electron beam and E-field of certain cavity modes in a coaxial cavity vircator is analyzed in this paper. According to the

https://doi.org/10.1017/S0022377807006976 Published online by Cambridge University Press

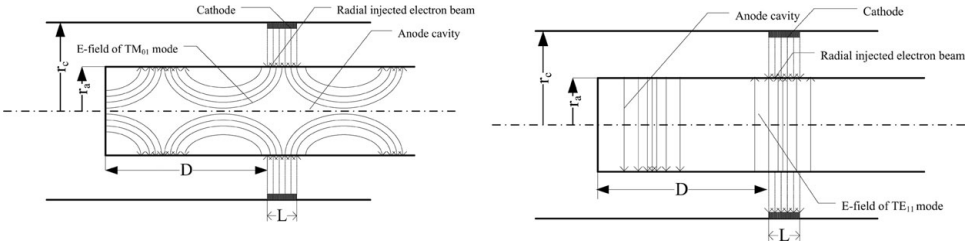


Figure 1. The coupling between radial injected electron beam and E-field of TE_{11} and TM_{01} modes.

E-field distribution pattern of operating modes in a beam–wave oscillating cavity, the resonating band between the injected electron beam and a certain cavity mode is obtained. The main frequency of virtual cathode oscillation is deduced. According to the double-frequency determination mechanism, a high-efficiency design and optimization method is proposed. Finally, the experimental results are given.

2. Frequency of beam–wave interaction in anode cavity

Generally, only the lowest two modes, TE_{11} and TM_{01}, are permitted to be the operating modes inside the cylindrical anode cavity for suppressing modes competition; high-order modes are cut off in the cavity and output waveguide. The coupling patterns between the radial injected electron beam and E-field of TE_{11} and TM_{01} modes are shown in Fig. 1.

In fact, any position along the axial electron beam injecting region on anode surface can be treated as an exciting point for beam power transformation to electromagnetic (EM) wave power. Consequently, we have

$$D + l = n\frac{\lambda}{2} + \frac{\lambda}{4} \quad (0 < l < L,\ n = 0, 1, 2, 3, \ldots) \tag{2.1}$$

where λ is the wavelength of operating mode inside anode cavity. According to (2.1) and Fig. 1, the wavelength of the operating modes inside the anode cavity determined by shifting the exciting point from left to right along the axial direction of electron beam injecting region can be given as

$$\frac{4D}{2n+1} < \lambda < \frac{4(D+L)}{2n+1}, \tag{2.2}$$

which corresponds to a frequency band

$$\Delta f = \frac{v_p(2n+1)}{4}\left(\frac{1}{D} - \frac{1}{D+L}\right), \tag{2.3}$$

where v_p is the phase velocity of waveguide mode.

Within the frequency band defined in (2.3), interaction between the injected electron beam and cavity mode can occur. The center frequency corresponding to the axial midpoint of the electron injecting region is

$$f_0 = \frac{v_p(2n+1)}{4(D + L/2)}. \tag{2.4}$$

Here, f_0 must be over the cutoff frequency of TE_{11} and TM_{01} modes, which will ensure that they are travelling modes in the output waveguide. The cutoff

https://doi.org/10.1017/S0022377807006976 Published online by Cambridge University Press

Table 1. Values of Δf and f_0 for different n.

n	0	1	2	3	4
Δf (GHz)	0.75–1.07	2.25–3.21	3.75–5.36	5.25–7.5	6.75–9.64
f_0 (GHz)	0.88	2.65	4.41	6.17	7.94

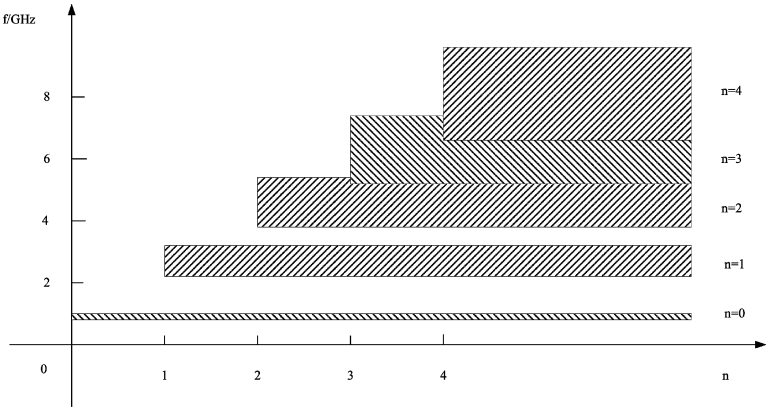


Figure 2. Schematic view of the resonant band (Δf) in a cavity coaxial vircator.

frequencies of TE_{11} and TM_{01} are, respectively, $f_{c-TE_{11}} = 2.405v_p/2\pi a$ and $f_{c-TM_{11}} = 1.841v_p/2\pi a$.

For instance, we take a group of parameters as follows: $a = 5.0$ cm, $D = 7.0$ cm and $L = 3.0$ cm. For different n, the frequency band defined by (2.3) and the center frequency given by (2.4) can be obtained as listed in Table 1. The Δf given in Table 1 can also be shown as a horizontal bar chart as in Fig. 2.

According to the coupling process of the electron beam and E-field of cavity modes shown in Fig. 1, it can be easily understood that the resonant frequency of electron beam–EM wave interaction inside anode cavity will tend to approach f_0, in other words, the midpoint of electron injecting region is inclining to be the center point of the wave node of operating modes. It also implies that the highest coupling efficiency will occur at this time. Figure 2 indicates that the adjacent resonant bands overlap after $n \geqslant 2$. Hence, if the operating frequency is chosen in the overlapped band, the frequency will probably shift in the HPM pulse duration, which will lead to the oscillation mechanism breakdown and modes competition. Therefore, the optimal operating frequency should be confined in the non-overlapped frequency bands or the bands with only upper edge overlap, for example, the frequency band corresponding to $n = 2$ in Fig. 2.

For the above given parameters, the frequency bands satisfy the frequency stable requirement only when $n = 0, 1, 2$. Meanwhile, the cutoff frequencies of TM_{01} and TE_{11} modes are, respectively, 2.3 and 1.76 GHz. So the operating frequencies can only be chosen from the f_0 corresponding to $n = 1$ or 2, namely, the optimal choice should be 2.64 or 4.41 GHz.

Considering that the TE_{11} mode is the lowest in the circular waveguide and has a strong radial E-field component, the modes competition tends to enhance the TE_{11} component in overall EM power. Meanwhile, the radially injected electron

https://doi.org/10.1017/S0022377807006976 Published online by Cambridge University Press

beam in a coaxial vircator generates the oscillating EM fields with radial E-field component stronger than other directions. Hence, it can be expected that the TE_{11} mode will dominate the interaction process between the injected electron beam and the EM wave inside the anode cavity. Moreover, misalignment on the axes of anode and cathode ring in the experimental geometry is unavoidable, the non-uniform electron emission will inevitably occur, which will lead to the enhancement of the TE_{11} mode. Hence, it will further enhance the coupling between the TE_{11} mode and the electron beam.

3. Main frequency of virtual cathode oscillation in a coaxial vircator

Supposing that electron movement in the coaxial diode and radial drift region is only along the radial direction with zero initial velocity and stable initial beam density, the E-field induced by the space charge inside the diode gap and anode cavity is described by a Poisson equation as

$$\nabla \cdot \mathbf{E} = \frac{\rho}{\varepsilon_0}, \tag{3.1}$$

where ρ and ε_0 are, respectively, the charge density and conductivity in vacuum.

Expanding (3.1) on cylindrical coordinates gives

$$\nabla \cdot \mathbf{E} = \frac{1}{r} \cdot \frac{d}{dr}(\mathbf{r} \cdot \mathbf{E}) = \frac{\rho}{\varepsilon_0}. \tag{3.2}$$

Substituting $\rho = -ne$ into (3.2) gives

$$\frac{1}{r} \cdot \frac{d}{dr}(\mathbf{r} \cdot \mathbf{E}) = \frac{ne}{\varepsilon_0}. \tag{3.3}$$

Here n and e are, respectively, the electron density and electron charge.

From Maxwell equations, we have

$$\nabla \times \mathbf{B} = \mu_0 \mathbf{j} + \mu_0 \varepsilon_0 \frac{d\mathbf{E}}{dt}, \tag{3.4}$$

where μ_0 and $\mathbf{j}$ are, respectively, the permeability and current density.

Under the steady-state hypothesis, we have $d\mathbf{E}/dt = 0$. The divergence of (3.4) gives

$$\nabla \cdot \mathbf{j} = \frac{1}{r} \cdot \frac{d}{dr}(\mathbf{r} \cdot \mathbf{j}) = 0. \tag{3.5}$$

Consequently,

$$\mathbf{j} = \frac{I_n}{2\pi r}\hat{r}. \tag{3.6}$$

Here I_n is radial beam current per unit length along the axial direction.

Supposing that a steady state exists when the virtual cathode forms with a potential of $\phi(r_c) = -V_0$ at a fixed position, and the reflected electrons have zero initial velocity and the anode potential is zero. Substituting $j = -nev$, and (3.6) into (3.3) it becomes

$$\frac{d(\mathbf{r} \cdot \mathbf{E})}{dr} = \frac{I_n}{2\pi\varepsilon_0 v}. \tag{3.7}$$

https://doi.org/10.1017/S0022377807006976 Published online by Cambridge University Press

Letting $F = \mathbf{r} \cdot \mathbf{E}$ and substituting $v = c \cdot (\gamma^2 - 1)^{1/2}/\gamma$ into (3.7), we obtain

$$\frac{dF}{dr} = \frac{I_n}{2\pi\varepsilon_0 v} = \frac{I_n}{2\pi\varepsilon_0 c} \cdot \frac{\gamma}{(\gamma^2 - 1)^{1/2}}. \tag{3.8}$$

With $\gamma(r) = 1 + e[\phi(r) + V_0]/m_0c^2$, (3.8) can be changed to

$$F\,dF = -\frac{I_n m_0 c}{2\pi\varepsilon_0 e} \cdot r \cdot \frac{\gamma}{(\gamma^2 - 1)^{1/2}}\,d\gamma. \tag{3.9}$$

The integration (3.9) from r_{vco} (radius of the virtual cathode) to r_{a} (radius of the anode) gives

$$\int_0^{V_a} F\,dF = -\frac{I_n m_0 c}{2\pi\varepsilon_0 e} \cdot \int_1^{\gamma} r\,d(\gamma^2 - 1)^{1/2}. \tag{3.10}$$

For a coaxial vircator system with anode radius greater than the diode gap, that is, $r_{\mathrm{a}} > 3(r_{\mathrm{c}} - r_{\mathrm{a}})$, $F(r)$ can be approximately given as

$$F(r) \approx \left(\frac{I_n m_0 c}{\pi\varepsilon_0 e}\right)^{1/2} \cdot [\gamma(r)^2 - 1]^{1/4} \cdot r^{1/2}. \tag{3.11}$$

Here r_{c} and r_{a} are, respectively, the cathode and anode radius.

According to (3.11), the potential distribution function in the electron drift region is

$$\frac{d\phi(r)}{dr} = -\left(\frac{I_n m_0 c}{\pi\varepsilon_0 e}\right)^{1/2} \cdot [(1 + \gamma(r))^2 - 1]^{1/4} \cdot r^{-1/2}, \tag{3.12}$$

where $\phi(r)$ is potential function inside the anode cavity.

Considering the boundary conditions and integrating (3.12), we have

$$\frac{2^{3/4}}{3}\left\{\frac{\varphi(2 + M\varphi)^{1/4}\Pi[\frac{3}{4}, \frac{1}{4}, \frac{7}{4}, -(M/2)\varphi]}{\{M\varphi[2 + M\varphi]\}^{1/4}} - \frac{(2 + M)^{1/4}\Pi[\frac{3}{4}, \frac{1}{4}, \frac{7}{4}, -M/2]}{[M(2 + M)]^{1/2}}\right\}$$
$$= (I_n N)^{1/2}(\sqrt{r} - \sqrt{r_{\mathrm{vco}}}), \tag{3.13}$$

where r_{vco} is radius of virtual cathode, $M = e/m_0c^2$, $N = m_0c/\pi\varepsilon_0 e$, $\varphi = \phi(r) + V_0$. Here $\Pi(\alpha, \beta, \xi, z)$ is a Gaussian hypergeometric function with a form

$$\Pi(\alpha, \beta, \xi, z) = \frac{\Gamma(\xi)}{\Gamma(\alpha)\Gamma(\beta)} \sum_{n=0}^{\infty} \frac{\Gamma(n + \alpha)\Gamma(n + \beta)}{\Gamma(n + \xi)} \frac{z^n}{n!} \quad (|z| < 1, \xi \neq 0, -1, -2, \ldots). \tag{3.14}$$

Equation (3.13) gives an approximate relation of the diode current, voltage and geometry parameters in the coaxial vircator system.

Assuming that the cathode has a longitudinal length of L, from (3.13) we can obtain the one-dimensional space-charge-limiting current for the radial electron drift region,

$$I_{\mathrm{splc}} = I_n L = \frac{2\sqrt{2}L}{9N(\sqrt{r} - \sqrt{r_{\mathrm{vco}}})^2}$$
$$\cdot \left\{\frac{\varphi(2 + M\varphi)^{1/4}\Pi[\frac{3}{4}, \frac{1}{4}, \frac{7}{4}, -(M/2)\varphi]}{[M\varphi(2 + M\varphi)]^{1/4}} - \frac{(2 + M)^{1/4}\Pi[\frac{3}{4}, \frac{1}{4}, \frac{7}{4}, -M/2]}{[M(2 + M)]^{1/2}}\right\}^2. \tag{3.15}$$

https://doi.org/10.1017/S0022377807006976 Published online by Cambridge University Press

In fact, for the non-relativistic case, (3.15) can be reduced to the form given by classical Langmuir–Blodgett law as

$$j_{\mathrm{a}} = \frac{4\varepsilon_0}{9}\sqrt{\frac{2e}{\gamma_0 m_0}}\frac{V_0^{3/2}}{r_{\mathrm{a}}^2\beta^2}, \tag{3.16}$$

where j_{a} is the current density on the anode surface and β is the relativistic factor, $\beta = v/c$.

When the reflected electron moves to the anode, we have $dt = dr/v$. Substituting it into (3.7), we obtain

$$dt = -\frac{2\pi\varepsilon_0}{I_n}\,dF. \tag{3.17}$$

Supposing that the reflected electron reaches the anode at $t = \bar{\tau}$, integrating (3.17) gives

$$\bar{\tau} = \int_{r_{\mathrm{vco}}}^{r_{\mathrm{a}}}\frac{dr}{v} = \frac{2\pi\varepsilon_0}{I_n}F(r_{\mathrm{a}}). \tag{3.18}$$

Substituting $I_n = 2\pi r_{\mathrm{a}} j_{\mathrm{a}}$, $j_{\mathrm{a}} = en_0 v(r_{\mathrm{a}}) = en_0 c(\gamma_0^2 - 1)^{1/2}/\gamma_0$ into (3.18), we have

$$\bar{\tau} = \left(\frac{2\varepsilon_0 m_0 c}{j_{\mathrm{a}} e}\right)^{1/2}(\gamma^2 - 1)^{1/4}, \tag{3.19}$$

where γ_0, n_0 are, respectively, the relativistic factors of injected electrons and electron density.

Letting $\gamma_0^2 - 1 \approx 2(\gamma_0 - 1)$ and introducing a relativistic correction to the electron mass, $m_0 \mapsto \gamma_0 m_0$, (3.19) reduces to

$$\bar{\tau} \approx \left(\frac{2\sqrt{2}\varepsilon_0\gamma_0 m_0 c}{j_{\mathrm{a}} e}\right)^{1/2}(\gamma_0^2 - 1)^{1/4} = \frac{\sqrt{2}}{\omega_{\mathrm{p}}}. \tag{3.20}$$

Equation (3.20) gives an approximate form of (3.19), which can be used in the relativistic case to evaluate the frequency of the reflected electron oscillation.

In the analysis above, the electron beam current is assumed to be purely radial with space-charge spreading being ignored, and the electrons flow inside the coaxial vircator is phase and density stable. That is, the potential at the virtual cathode will be undisturbed and keeps an unsteady-state balance [2].

Considering the energy conversion owing to the interaction between injected electron beam and EM wave inside the anode cavity, the electron will be velocity modulated before arriving at the virtual cathode, which will result in virtual cathode potential fluctuation. After that, this potential fluctuation leads to oscillation of the reflected electron beam current. Meanwhile, the transmitted electron beam current emerges in this case, which is different from the initial state of total reflection.

Supposing that the potential oscillation of the virtual cathode and the induced reflected current modulation are formed, the injecting current modulation will be aroused by the reflected current modulation.

In the following, we discuss the relationship between the oscillation of the reflected electron and that of the virtual cathode potential.

On the assumption that the potential fluctuation of the virtual cathode starts at time t_1, it results in the shift of potential from $-V_0$ to $\phi_{\mathrm{vco}}(t_1) = -V_0 + \Delta V$ and the reflected electron beam density from Q_0 to $Q_0 - \Delta Q$. After a time duration $\bar{\tau}$, the electron beam bunch with decreased density reaches the anode and leads to the

https://doi.org/10.1017/S0022377807006976 Published online by Cambridge University Press

injected electron beam density changing from Q_0 to $Q_0 + \Delta Q$. After the next $\bar{\tau}$, that density increased electron beam bunch reaches the virtual cathode and ignites the next circle of potential oscillation [10].

The oscillations of the reflected electron and virtual cathode have a comparative basis with the Barkhausen–Kurz oscillator. So, the oscillations of the virtual cathode and modulated beam current present the same frequency with a oscillation period of $2\bar{\tau}$, which is equal to the half period of the reflected electron motion, that is,

$$f_{\mathrm{vco}} = f_{\mathrm{em}} = \frac{1}{2\bar{\tau}}, \tag{3.21}$$

where $\bar{\tau}$ is the average electrons transit time from the virtual cathode to the anode given by (3.19), f_{vco} and f_{em} are, respectively, the oscillating frequency of the virtual cathode and modulated injecting beam current.

The previous discussion also implies that the frequency of the modulated injecting beam current determines the energy conversion frequency during the beam–wave interaction process, which is also the induced EM wave frequency in the coaxial vircator. Therefore, the main frequency of beam–wave interaction, namely, the main frequency of the generated HPM, can be obtained by substituting (3.16) and (3.19) into (3.21) as

$$f_{\mathrm{vco}} = \frac{1}{6(\sqrt{r_{\mathrm{c}}} - \sqrt{r_{\mathrm{a}}})}\left(\frac{e}{\sqrt{2}\pi N r_{\mathrm{a}}\varepsilon_0 m_0 c}\right)^{1/2}[(1+MV_0)^2 - 1]{-}1/4 \cdot \left\{\frac{V_0(2+MV_0)^{1/4}\Pi[\frac{3}{4},\frac{1}{4},\frac{7}{4},-(M/2)V_0]}{[MV_0(2+MV_0)]^{1/4}} - \frac{(2+M)^{1/4}\Pi[\frac{3}{4},\frac{1}{4},\frac{7}{4},-(M/2)]}{[M(2+M)]^{1/2}}\right\}. \tag{3.22}$$

Equation (3.22) gives the main frequency of the generated HPM inside the coaxial vircator with an explicit form, by which we can easily estimate the operating frequency of the experimental configuration with geometry and input parameters. Also, we can roughly calculate the frequency by substituting (3.20) into (3.21).

4. High-efficiency coaxial vircator design

Generally, high efficiency is closely interrelated with a narrow frequency band for most HPM generators. There is no exception for the vircator. In order to attain high efficiency, vircator systems should operate with a narrow frequency band. According to the discussions in Secs 2 and 3, two mechanisms of oscillation exist in a coaxial vircator; the first is the modulated injecting beam current oscillation whose frequency is equal to that of virtual cathode oscillation; and the other is the oscillation of the induced EM wave of certain modes corresponding to the resonant frequency band. This oscillation mechanism is different from the prevenient viewpoint that the double-frequency characteristic of a vircator is aroused by the different frequencies of the virtual cathode and the reflected electron beam current, which has been the dominant view of the HPM research community until recently [11].

From this point of view, if we intend to design a high-efficiency coaxial vircator system, a fundamental principle is to let the oscillating frequency of the virtual cathode be approximately equal to the center frequency f_0. A large difference between these two frequencies will lead to wideband or double-frequency output and low efficiency.

https://doi.org/10.1017/S0022377807006976 Published online by Cambridge University Press

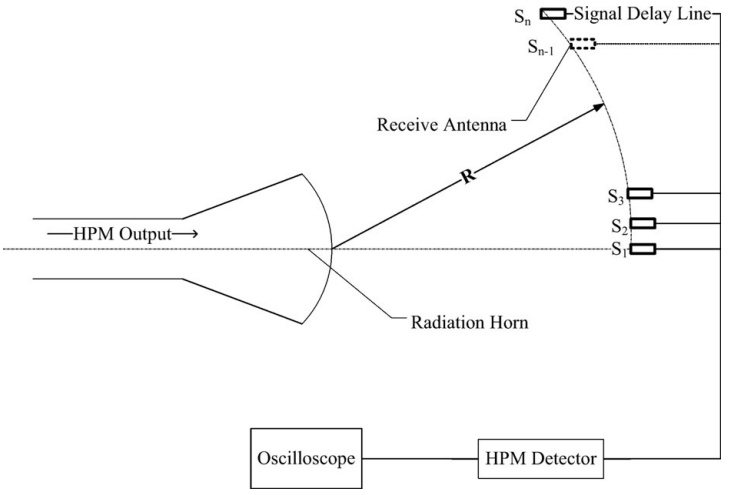


Figure 3. Schematic diagram of HPM power measurement.

We assume a coaxial vircator with the following parameters, the diode voltage is 500 kV, cathode and anode radii are, respectively, 7.0 cm and 5.0 cm. From (3.22), we can obtain the main frequency of the virtual cathode as 2.57 GHz, which is close to $f_0 - 2.65$ GHz corresponding to $n = 1$ in Table 1. To obtain a high-efficiency HPM generation, we should adjust one of them to approach another, and finally make the system operating under a single frequency.

Here f_0 can be shifted by adjusting D or L as shown in Fig. 1. Based on the given parameters, when $n = 1$, by adjusting D to 7.2 cm, f_0 changes to 2.57 GHz.

Meanwhile, by substituting (3.20) into (3.21), it also gives $f_{\text{vco}} = 2.577$ GHz, which is in accordance with the result from (3.22).

The above analysis describes a design process for a high-efficiency coaxial vircator under certain geometry and input parameters. It is based on the one-dimensional electron emission and movement hypothesis, and the validity still needs to be testified experimentally.

5. Experimental results of the high-efficiency coaxial vircator

Based on the analysis in Secs 2, 3 and 4, a coaxial vircator experiment system has been designed and tested on the MC-55 HV pulse generator, which is designed and built with a 10 Ω transmission line and a diode voltage of 400–600 kV. Generated HPM power is measured by the method of radiation field integration as shown in Fig. 3. The experimental system and HPM power detector are shown in Fig. 4. According to the output voltage of the high-voltage generator and high-efficiency prediction parameters given in Sec. 4, the system operating frequency is designed at approximately 2.6 GHz.

The typical experimental result of a high-efficiency coaxial vircator is shown in Fig. 5. The relationship between D and power efficiency obtained is given in Fig. 6.

Figure 6 indicates that the highest efficiency is obtained near $D = 7.2$ cm, which is consistent with that given by the theoretical design in Sec. 4. A maximal output power of 1.23 GW is obtained by radiation field integration under a 480 kV diode voltage and 29.5 kA diode current, which gives a power efficiency of 8.7%. The

https://doi.org/10.1017/S0022377807006976 Published online by Cambridge University Press

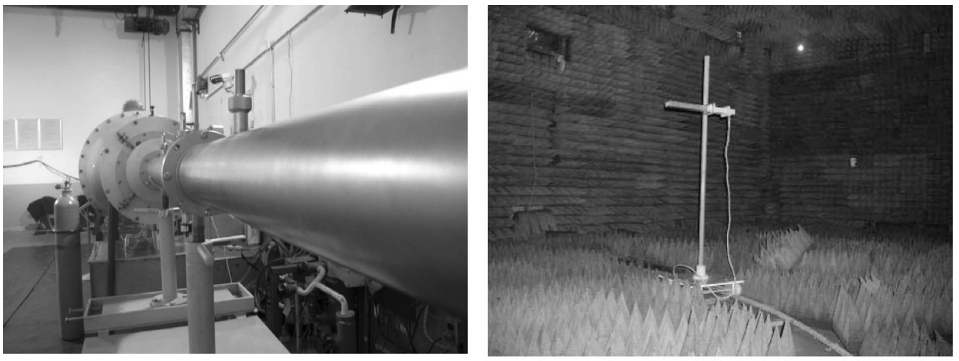


Figure 4. Experimental setup of (a) the coaxial vircator and (b) the HPM power detector.

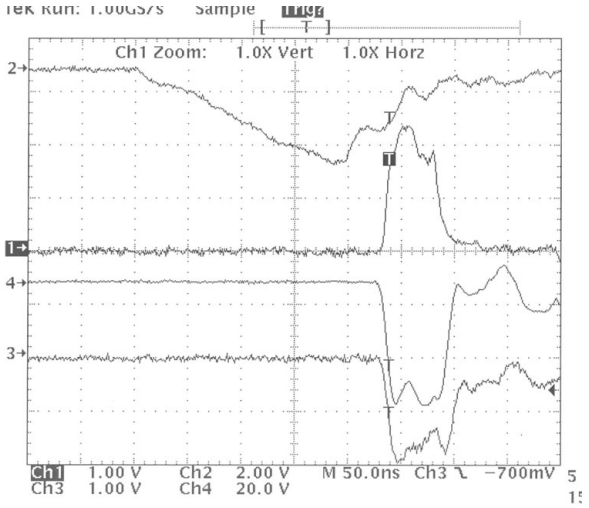


Figure 5. Typical experimental result of a high-efficiency coaxial vircator (CH2: voltage on pulse forming line, 310 kV/V; CH3: diode voltage, 300 kV/V; CH4: diode current, 670 A/V; CH1: HPM pulse, 500 MW/V).

diode current and voltage are measured with a Rogowski coil and capacity divider, respectively. HPM power detector array is settled along an arc with a radius of R as shown in Fig. 3. Each detector is connected with the same open-ended waveguide antenna; the HPM signal from each channel is discriminated by the different length of the signal delay line and finally recorded with an oscilloscope. Meanwhile, another power measurement method is also introduced for comparison by moving a single detector along the same arc. By recording the power density of a series of shots as well as keeping another detector fixed for normalization, the total radiation power is calculated by integrating the power density at the detector over the spherical surface as

$$P_{\mathrm{r}} = \sum_{i=1}^{n-1} A_n (S_n + S_{n+1})/2 = 1.23 \text{ GW}. \tag{5.1}$$

https://doi.org/10.1017/S0022377807006976 Published online by Cambridge University Press

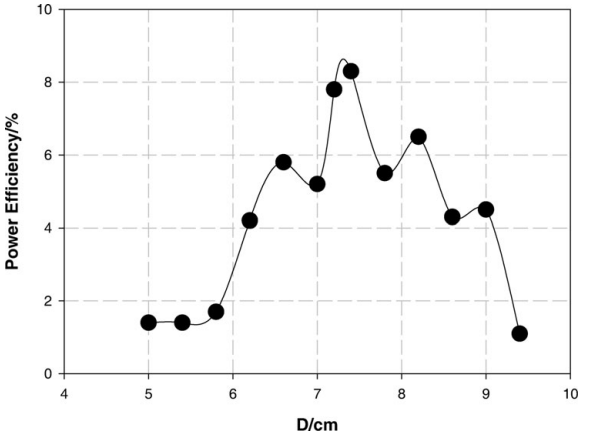


Figure 6. Power efficiency versus D.

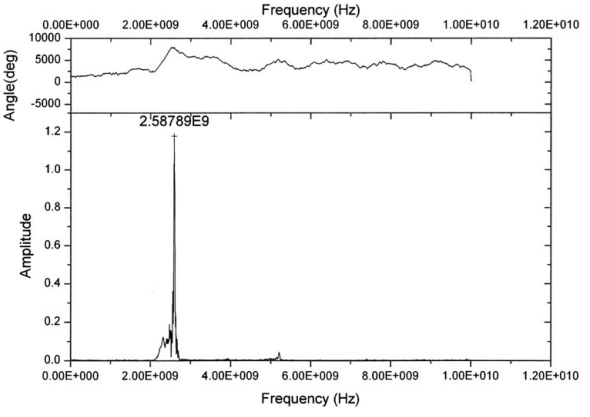


Figure 7. Spectrum of radiation of the HPM pulse.

Here A_n is the flank area between two neighboring point and S_n is the power density at the entrance boundary of receiving antenna.

A degassing and coating process is introduced to improve the performance of the cathode and anode, and the different material of the cathode and anode is also tested. The pulse shortening effect is depressed for a 55 ns electron beam injection in the experiment, and the HPM pulse width is approximately equal to that of the beam current. Hence, the energy efficiency is obtained as high as 6.8%.

The optimal operating frequency of the experimental system is chosen at 2.57 GHz according to the discussion in Sec. 4. After a small range adjustment of certain parameters, a frequency and phase stable HPM output is obtained as shown in Fig. 7. The main frequency is at 2.59 GHz and remains stable (shown in Fig. 8) during the output HPM pulse. The recess on the pulse envelope is probably caused by HPM breakdown on the surface of radiation antenna.

https://doi.org/10.1017/S0022377807006976 Published online by Cambridge University Press

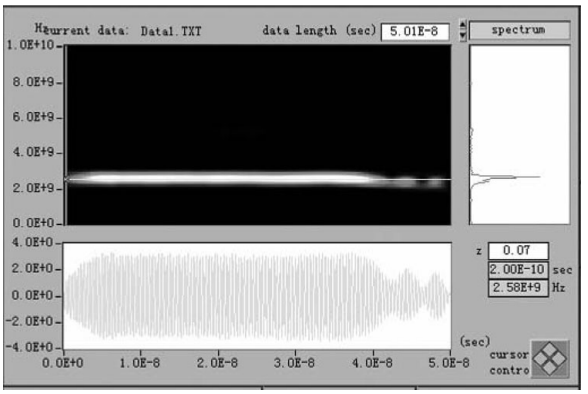


Figure 8. Joint time–frequency analysis of the output HPM pulse.

6. Conclusion

For the coaxial vircator operated with the lowest two modes, there exists a series of resonant frequency bands that determine the coupling process of the radial injected electron beam and cavity modes. The operating frequency tends to approach the center frequency of such bands. The frequency of the virtual cathode oscillation can be approximately given as half the reflected electron oscillation. A design and optimization method of a coaxial cavity vircator system has been given according to the discussion of resonant frequency bands and the oscillating frequency of the virtual cathode. An experimental system has been built and tested. With a HPM radiation power of 1.23 GW, power and energy efficiency, respectively, of 8.7% and 6.8% are obtained. The effect of anode cavity length on efficiency obtained in the experiment is accordance with the analysis given in Sec. 2. The pulse shortening is depressed by introducing a new material and degassing process of anode and cathode. The measured HPM pulse width is 50 ns, which is approximately equal to the pulse length of the electron beam current.

References

[1] Benford, J. and Swegle, J. 1992 *High-Power Microwaves*. Artech House, Norwood, MA, pp. 345–387.

[2] Sullivan, D. J., Walsh, J. E. and Coutsias, E. A. 1987 Virtual cathode oscillator (Vircator) theory. *High Power Microwave Sources* (ed. V. Granatstein and I. Alexeff). Artech House, Norwood, MA, pp. 441–487.

[3] Zherlitsyn, A. G. 1990 Microwave generation by triode with coaxial-type virtual cathode. *Pisma Zh. Tekh. Fiz* **16**(2), 78–80.

[4] Liu, G. Z. et al. 1997 Study on coaxial diode and vircator. *Proc. SPIE Intense Microwave Pulses V*, SPIE, Philadelphia, PA, pp. 230–237.

[5] Crawford, M., Kristiansen, M. and Hatfield, L. L. 1993 Cylindrically-symmetric virtual cathode oscillator high power microwave source. *Proc. 9th IEEE Int. Conf. on Pulsed Power*, Albuquerque, NM, pp. 608–614.

[6] Crawford, M., Kristiansen, M. and Hatfield L. L. 1995 Experimental results from a coaxial vircator. *Proc. IEEE Int. Conf. on Plasma Science*, p. 232.

[7] Jiang, W., Woolverton, K., Dickens, J. and Kristiansen, M. 1999 High power microwave generation by a coaxial virtual cathode oscillator. *IEEE Trans. Plasma Sci.* **27**(6), 1538–1542.

https://doi.org/10.1017/S0022377807006976 Published online by Cambridge University Press

[8] Jiang, W., Woolverton, K., Dickens, J. and Kristiansen, M. 1999 Optimization of microwave generation by coaxial vircator. *Proc. IEEE International Conference on Plasma Science*, Monterey, CA, p. 328.

[9] Choi, E. H. et al. 2003 Power efficiency enhancement of a coaxial virtual cathode oscillator with ring-type reflector. *Proc. IEEE 30th Int. Conf. on Vacuum Electronics*, p. 341.

[10] Jiang, W., Masugata, K. and Yatsui K. 1995 Mechanism of microwave generation by virtual cathode oscillation. *Phys. Plasma* **2**(3), 982–986.

[11] Chung, M. 2004 Comparison of recent high efficiency vircator. *Proc. 31st IEEE Int. Conf. on Plasma Science*, p. 279.

https://doi.org/10.1017/S0022377807006976 Published online by Cambridge University Press